

# Production of cold formaldehyde molecules for study and control of chemical reaction dynamics with hydroxyl radicals

Eric R. Hudson, Christopher Ticknor, Brian C. Sawyer, Craig A. Taatjes,\*

H. J. Lewandowski, J. R. Bochinski,<sup>†</sup> John L. Bohn, and Jun Ye

JILA, National Institute of Standards and Technology and University of Colorado,

Department of Physics, University of Colorado, Boulder, CO 80309-0440 <sup>‡</sup>

(Dated: September 26, 2018)

We propose a method for controlling a class of low temperature chemical reactions. Specifically, we show the hydrogen abstraction channel in the reaction of formaldehyde ( $\text{H}_2\text{CO}$ ) and the hydroxyl radical ( $\text{OH}$ ) can be controlled through either the molecular state or an external electric field. We also outline experiments for investigating and demonstrating control over this important reaction. To this end, we report the first Stark deceleration of the  $\text{H}_2\text{CO}$  molecule. We have decelerated a molecular beam of  $\text{H}_2\text{CO}$  essentially to rest, producing cold molecule packets at a temperature of 100 mK with a few million molecules in the packet at a density of  $\sim 10^6 \text{ cm}^{-3}$ .

PACS numbers: 82.20.-w, 33.80.Ps, 39.10.+j, 32.60.+i

Recent exciting developments in ultracold matter research include the creation of ultracold molecules by magneto-association [1], leading to molecular Bose-Einstein condensation [2]. Despite the rich physics demonstrated in these systems, all are characterized by spherically symmetric interactions whose effect is included through one parameter, namely the s-wave scattering length. By contrast, the permanent electric dipole moment possessed by polar molecules permits long-range and anisotropic interactions and enables new methods for external control in an ultra-cold environment [3]. The electric dipole-dipole interaction (and control over it) gives rise to unique physics and chemistry including novel collision and chemical reaction dynamics. Lack of spherical symmetry in the interaction causes colliding molecules to be attracted or repelled depending on their relative orientation. Thus, an external electric field, which orients the molecules, will have a profound effect on the molecular interactions [4]. Furthermore, because the transition states of a chemical reaction often involve specific orientations of the molecular dipoles, an external electric field may shift the energy barrier to reaction, making a particular reaction pathway more or less favorable. A Stark decelerator [5, 6, 7] producing cold polar molecules with tunable and well-defined translational energy is thus an ideal tool for the study of low (or negative) barrier chemical reactions. We note other experiments utilizing photo-association [8, 9, 10] have succeeded in producing ultra-cold heteronuclear alkali dimers.

In this letter, we present a study of the collision and reaction properties of  $\text{OH}$  with  $\text{H}_2\text{CO}$  at low temperatures, followed by a detailed description of experiments required and carried out so far to probe these novel dynamics. The calculations suggest for the first time that chemical reactions, as well as collision cross sections, can be altered orders of magnitude by varying either the molecular state, or external electric field strength. We specifically consider the H-abstraction channel in the re-

action of  $\text{H}_2\text{CO}$  and  $\text{OH}$ :  $\text{H}_2\text{CO} + \text{OH} \rightarrow \text{CHO} + \text{H}_2\text{O}$ . This reaction not only represents a key component in the combustion of hydrocarbons, but also plays an important role in atmospheric chemistry where it is the primary process responsible for the removal of the pollutant,  $\text{H}_2\text{CO}$  [11, 12, 13, 14, 15, 16, 17]. Near room temperature the rate of this reaction is weakly dependent on temperature, suggesting the barrier to the process (if any) is very low [13]. Measurements of the thermal activation energy,  $E_a$ , are inconclusive [11, 12, 13, 14, 15, 16, 18], ranging from  $E_a/R = 750 \text{ K}$  to  $-931 \text{ K}$ , with the most recent measurement giving a value of  $-135 \text{ K}$  [18]. Here  $R$  is the universal gas constant. The most accurate calculations [19] predict the energy of the transition state for the abstraction to lie between  $-700 \text{ K}$  and  $+60 \text{ K}$  relative to the reactants.

Experimentally, both  $\text{OH}$  [6, 7, 20] and  $\text{H}_2\text{CO}$  (this work) molecules have been produced at low temperatures via Stark deceleration. In the case of spontaneous reaction ( $E_a < 0$ ) [11, 13, 15, 16], by magnetically trapping  $\text{OH}$  in the presence of a tunable bias electric field and “bombarding” the trap with decelerated  $\text{H}_2\text{CO}$  packets the  $\text{OH} - \text{H}_2\text{CO}$  total scattering and reaction rates can be mapped as a function of collision energy and applied electric field. Thus  $E_a$  can be measured. If  $E_a > 0$ , as some measurements and theory suggest [12, 14, 17, 19], the collision energy tuning afforded by the Stark decelerator provides a direct way to measure the energy barrier to reaction. Unlike thermal kinetics studies, which rely on fitting the Arrhenius formula to reaction rates, the Stark decelerator can be used to tune the collision energy above and below the threshold energy.

As shown in Fig. 1(a),  $\text{H}_2\text{CO}$  is a near-symmetric prolate top molecule, with nearly degenerate rotations about the b- and c- axes. The dipole moment,  $\mu_a$ , along the a-axis causes these nearly degenerate, opposite parity states to experience a large Stark shift with an applied electric field, as shown in Fig. 1(b-d). Here, the states

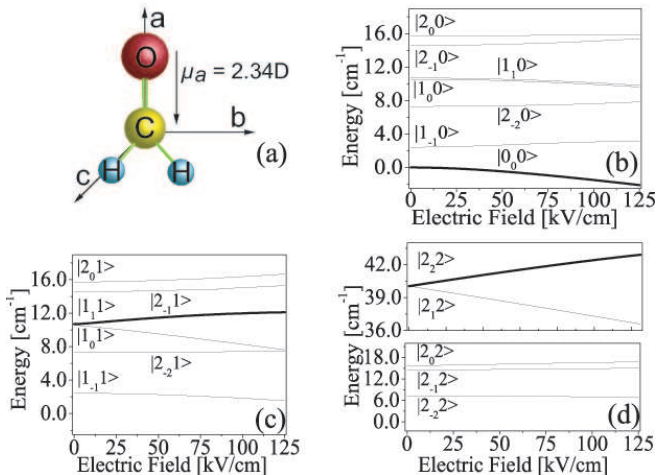


FIG. 1: (a) (Color online) H<sub>2</sub>CO. (b-c) Stark shifts of the low-lying rotational states of H<sub>2</sub>CO. States of interest for this work are shown in bold.

are labeled by their zero-field identity in the  $|J_\tau m_J >$  basis, where  $\tau = K_a - K_c$  ( $K_i$  is the projection of  $J$  along the  $i$ th axis) [21]. Of particular interest to this work is the  $|1_1 1 >$  state (Fig. 1(c)), which is the upper component of the lowest  $J$  level of ortho-formaldehyde and is hence well populated in our supersonic expansion. This state experiences a large Stark shift ( $1.32 \text{ cm}^{-1}$  at  $125 \text{ kV/cm}$ ), making it excellent for Stark deceleration. There are other states accessible via, for example, stimulated Raman adiabatic passage that offer an improved Stark deceleration efficiency ( $|2_2 2 >$ ) or a good candidate for implementing an AC Stark trap ( $|0_0 0 >$ ) [22].

**OH-H<sub>2</sub>CO Theory.** The Hamiltonian,  $H$ , used in the scattering calculations takes the following form:

$$H = T + H_{OH} + H_{H_2CO} + H_{Stark} + H_{dd} + H_{sr} + H_{chem}. \quad (1)$$

Here  $T$  is the kinetic energy,  $H_{OH}$  and  $H_{H_2CO}$  are the Hamiltonians of the separated molecules, and  $H_{Stark}$  describes the action of the electric field on the individual molecules.  $H_{dd}$  represents the long-range dipole-dipole interaction between the molecules, which depends on the orientations of the molecules relative to the field axis, as well as the distance  $R$  between them. This will be expressed in a basis of molecular eigenstates (including the effect of the field), as was done in Ref. [4]. In addition, to prevent the dipole-dipole interaction from overwhelming the short-range interaction, we replace its  $1/R^3$  variation with  $1/(R^3 + c_{dd})$  for an appropriate constant  $c_{dd}$  [23]. The chemical reaction dynamics are modeled in a schematic way by the terms  $H_{sr}$  and  $H_{chem}$ . The goal of  $H_{sr}$  is to mimic an anisotropic interaction with a barrier, not necessarily to characterize the OH-H<sub>2</sub>CO system. This approximation is justified for the low reaction barrier where the dipole-dipole interaction dominates over internal molecular dynamics. Thus, we construct a po-

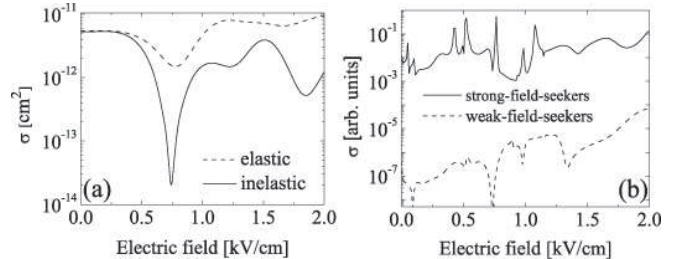


FIG. 2: (a) Computed elastic and inelastic OH - H<sub>2</sub>CO collision cross sections as a function of external electric field at 1 mK. (b) Chemical reaction cross sections from the schematic H-abstraction model.

tential as an expansion into Legendre functions,

$$H_{sr} = V_o(R) - 2V_2(R)C_{20}(\theta, \phi). \quad (2)$$

Here  $(\theta, \phi)$  represent the spherical angles of the relative coordinate between the molecules, referred to the electric field axis, and  $C_{20}$  is a reduced spherical harmonic [24]. The isotropic part of this potential carries the barrier at a radius  $R \approx R_b$ ,

$$V_o(R) = \frac{C_{12}}{R^{12}} - \frac{C_6}{R^6} + D_B \exp\left(\frac{-(R - R_b)^2}{w_b}\right). \quad (3)$$

The height of the barrier depending on  $D_B$  is fully adjustable with  $w_b$  characterizing the range. In the following, we set the barrier height equal to the threshold energy of the incoming molecule. The radial dependence of  $V_2$  is chosen to have a magnitude comparable to  $V_o$ , but to change sign as  $R$  crosses  $R_b$ . Thus the polar molecules attract in a head-to-tail configuration for  $R > R_b$ , but attract in a tail-to-tail configuration upon crossing the barrier. Finally, chemical reactivity ( $H_{chem}$ ) is modeled by coupling to a purely repulsive artificial channel. The coupling to this channel is represented by a decaying exponential in  $R$ , which is of negligible size for  $R > R_b$ . To complete a chemical reaction, the molecules must cross over the barrier, reverse their relative orientation, and find the artificial channel.

Collision cross sections for OH-H<sub>2</sub>CO scattering in this model are shown in Fig. 2(a). Here both molecules are assumed to be in spin-stretched, weak-field-seeking states:  $|Fm_F, parity > = |22, f >$  for OH, and  $|1_1 1 >$  for H<sub>2</sub>CO. The cross section for elastic (spin-changing) collisions is shown as a solid (dashed) line. The cross sections are large and comparable, and exhibit strong modulations as a function of an applied electric field. This has been explained for OH-OH scattering on the basis of purely long-range scattering by the dipole-dipole interaction [4]. Thus, these results are robust and independent of the detailed form of the short-range interaction.

The sensitive dependence of cold molecules on internal state and electric field engenders new prospects for probing and controlling the chemical reaction itself. To

illustrate this, we show in Fig. 2(b) the chemical reaction cross section versus electric field. The collision energy is assumed to be 1 mK. (Note that, because the reaction mechanism is schematic in our model we report only relative values for the cross sections.) The solid line is for collisions in which both OH and H<sub>2</sub>CO molecules are in their strong-field-seeking states. At this energy the field has a profound influence on the reaction cross section, mostly by accessing a very large number of resonant states. Considering that each resonant state spans a different region of configuration space, mapping out resonances such as these would serve as an extremely sensitive probe to transition states. The dashed trace in Fig. 2(b) shows the reaction rate for weak-field-seeking states of the reactants. In addition to probing many resonances, this cross section rises by nearly four orders of magnitude as the field increases. This rise is also a direct consequence of the dipole-dipole interaction. In Refs. [4, 25] it was shown that for polar molecules in weak-field-seeking states, the dipole-dipole interaction can “shield” these molecules from getting close enough together to react chemically. Thus the cross section is strongly suppressed relative to that for strong-field-seekers. However, as the field is increased, the inner turning point of the relevant potential curve moves to smaller  $R$ , making the shielding less effective, and hence, the reaction more likely.

While the above discussion is relevant for future studies in a low temperature trap environment, another important capability for current experiments is the direct control of the H-abstraction reaction barrier height through the application of an external electric field. The basic H-abstraction reaction mechanism, following Ref. [14], is shown in Fig. 3. We note that Ref. [26] presents a slightly different H-abstraction configuration, but with the same end-to-end dipole coupling scheme. During the H-abstraction process, the energy required to rotate one dipole moment (OH) versus the other (H<sub>2</sub>CO) enables our proposed control of reaction dynamics using an external electric field. Hence, the two abstraction configurations present no difference other than the magnitude of the shift we can create in the reaction barrier. The important characteristic to note is that the hydrogen-bonded complex (HBC) in the second panel (Fig. 3) forms along an attractive direction of the two electric dipoles, but in the transition state (TS) the OH dipole has essentially flipped its orientation relative to the H<sub>2</sub>CO dipole. While an external electric field, which orients the molecules would allow (and perhaps even encourage) the formation of the HBC; it would add an energy barrier to the formation of the TS, and thus the H-abstraction channel through the OH dipole-field interaction. Based on the bond geometries shown in Ref. [14], the addition to the energy barrier in going from the HBC to the TS is  $\approx 1.8\mu_{OH}|\vec{E}|$ , where  $\mu_{OH}$  is the expectation value of the dipole for the OH molecule. For a high, yet attainable, electric field of 250 kV/cm, the additional barrier energy

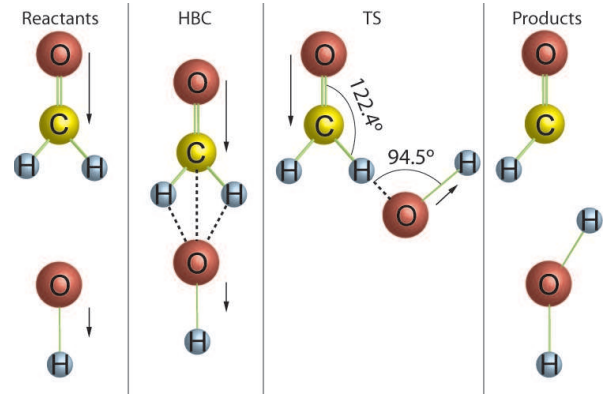


FIG. 3: (Color online) The reaction mechanism for the H-abstraction channel following Ref [14].

would be 10 K. Thus, assuming a reaction barrier at a H<sub>2</sub>CO collision speed of 223 m/s (60 K [19]) the applied electric field would shift the required collision velocity to 234 m/s, well within the Stark decelerator resolution.

**Experiment.** The decelerator used for H<sub>2</sub>CO is similar to the apparatus in our previously described OH experiments [6, 7, 27]. Molecules in a skinned, pulsed supersonic beam are focused by an electrostatic hexapole field to provide transverse coupling into the Stark decelerator. The Stark decelerator is constructed of 143 slowing stages spaced 5.461 mm apart with each stage comprised of two cylindrical electrodes of diameter 3.175 mm separated axially by 5.175 mm and oppositely biased at high voltage ( $\pm 12.5$  kV). Successive stages are oriented at 90° to each other to provide transverse guiding of the molecular beam. The geometry of the slowing stages provides an electric field maximum between the electrodes with the field decreasing away from the electrode center. Switching the electric field when the molecules are directly between two adjacent stages (no net deceleration) is denoted by a synchronous phase angle of  $\phi_o = 0^\circ$  (often referred to as bunching), while switching the electric field when the molecules are between the electrodes (maximum deceleration) is denoted by  $\phi_o = 90^\circ$ .

The H<sub>2</sub>CO molecules are produced from the cracking of the formaldehyde polymer to produce the monomer, which is passed through a double u-tube apparatus [28]. Xenon at 2 bar pressure is flowed over the collected H<sub>2</sub>CO, held at 196 K where H<sub>2</sub>CO has  $\sim 2.7$  kPa (20 Torr) vapor pressure. This Xe/H<sub>2</sub>CO mixture is expanded through a solenoid type supersonic valve producing a beam with a mean speed of 350 m/s with approximately a 10% velocity spread.

H<sub>2</sub>CO is detected using laser-induced fluorescence. The molecules are excited from the  $|1_11\rangle$  ground state by photons at 353 nm generated from a frequency-doubled, pulsed-dye laser pumped by Nd:YAG laser to the  $\tilde{A}^1A_2$  electronically excited state with one quantum in the  $\nu_4$  out-of-plane bending vibrational mode.

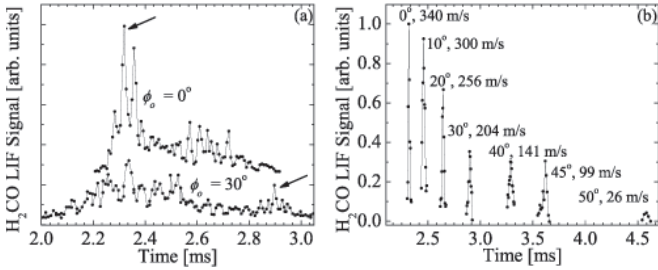


FIG. 4: Stark deceleration of  $\text{H}_2\text{CO}$  molecules, showing (a) bunching ( $\phi_o = 0^\circ$ ) and Stark deceleration at  $\phi_o = 30^\circ$  (offset down for clarity). (b) Stark decelerated packets of  $\text{H}_2\text{CO}$  molecules at the output of the decelerator.

Approximately 40% of the excited  $\text{H}_2\text{CO}$  decays non-radiatively [29], while the remaining molecules emit distributed fluorescence from 353 nm to 610 nm [30].

Shown in Fig. 4 are time-of-flight (ToF) measurements taken at the exit of the decelerator, which is  $\sim 0.9$  m down-stream from the valve. In these figures the time axis is relative to the beginning of deceleration. In Fig. 4(a) where the decelerator is operated at  $\phi_o = 0^\circ$ , a large peak in the ToF curve denotes the arrival (marked by an arrow) of the phase stable packet whose density is  $\sim 10^6$   $\text{cm}^{-3}$  and contains a few million molecules. It is important to note that even though the speed of this packet is 340 m/s, 10 m/s lower than the pulse mean speed, no deceleration has occurred. Instead the molecules in the pulse whose speed was in the range from  $340 \text{ m/s} \pm 25$  m/s were loaded into the packet as detailed in our earlier work [27]. Also shown in Fig. 4(a), but offset for clarity is the ToF curve for deceleration at  $\phi_o = 30^\circ$ . Here the arrow denotes the arrival of a slowed  $\text{H}_2\text{CO}$  packet with a mean velocity of 204 m/s. Displayed in Fig. 4(b) are ToF curves for the slowed molecular packets as a function of  $\phi_o$ . The minimum speed shown is 26 m/s for  $\phi_o = 50^\circ$ , resulting in a temperature of  $\sim 100$  mK.

To observe the OH- $\text{H}_2\text{CO}$  collision and reaction dynamics requires monitoring both the OH population and the production of the formyl radical (CHO). We have developed sensitive fluorescence imaging techniques for OH [7], and because CHO has a low ionization potential (8.1 eV), high signal-to-noise ratio photo-ionization detection of the reaction can be implemented. Nevertheless, given the current available densities of the reactants the observation of the dynamics proposed here will be daunting. However, further improvements such as multiple trap loading and secondary cooling of the molecular samples should make these observations possible.

In summary, we have detailed new methods to study interspecies molecular collision and reaction dynamics, and have shown how control of these processes may be achieved. We have also demonstrated preparation of both cold polar molecules required for these studies. Experiments are currently poised to begin exploring the rich

physics presented by the dipolar interaction.

Funding support for this work comes from NSF, NIST, DOE, and the Keck Foundation. CAT is supported by the Division of Chemical Sciences, Geosciences, and Biosciences, the Office of Basic Energy Sciences, the DOE.

\* JILA visiting fellow 2004. Permanent Address: Combustion Research Facility, Sandia National Laboratories, Livermore, CA 94551-0969

† Present Address: Department of Physics, North Carolina State University, Raleigh, NC 27695

‡ Electronic Address: Eric.Hudson@Colorado.edu

[1] E. A. Donley et al., *Nature* **417**, 529 (2002).

[2] M. Greiner, C. A. Regal, and D. S. Jin, *Nature* **426**, 537 (2003); M. W. Zwierlein et al., *Phys. Rev. Lett.* **91**, 250401 (2003); S. Jochim et al., *Science* **302**, 2101 (2003); T. Bourdel et al., *Phys. Rev. Lett.* **93**, 050401 (2003).

[3] Magnetic dipoles and electric quadrupoles also present anisotropic interactions. See A. Griesmaier et al., *Phys. Rev. Lett.* **94**, 160401 (2005) and R. Santra and C. H. Greene, *Phys. Rev. A* **67**, 062713 (2003), respectively.

[4] A. V. Avdeenkov and J. L. Bohn, *Phys. Rev. A* **66**, 052718 (2002); *ibid.* *Phys. Rev. Lett.* **90**, 043006 (2003).

[5] H. L. Bethlem, G. Berden, and G. Meijer, *Phys. Rev. Lett.* **83**, 1558 (1999).

[6] J. R. Bochinski et al., *Phys. Rev. Lett.* **91**, 243001 (2003).

[7] J. R. Bochinski et al., *Phys. Rev. A* **70**, 043410 (2004).

[8] D. Wang et al., *Phys. Rev. Lett.* **93**, 243005 (2003).

[9] A. J. Kerman et al., *Phys. Rev. Lett.* **92**, 033004 (2004).

[10] M. W. Mancini et al., *Phys. Rev. Lett.* **92**, 133203 (2004).

[11] E. D. Morris and H. Niki, *J. Chem. Phys.* **55**, 1991 (1971).

[12] M. R. Soto and M. Page, *J. Phys. Chem.* **94**, 3242 (1990).

[13] L. J. Stief et al., *J. Chem. Phys.* **73**, 2254 (1980).

[14] M. Dupuis and W. A. Lester, *J. Chem. Phys.* **81**, 847 (1984).

[15] H. Niki et al., *J. Phys. Chem.* **88**, 5342 (1984).

[16] R. A. Yetter et al., *J. Chem. Phys.* **91**, 4088 (1989).

[17] H. Y. Li et al., *Chem. Phys.* **307**, 35 (2004).

[18] V. Sivakumaran et al., *Phys. Chem. Chem. Phys.* **5**, 4821 (2003).

[19] B. D'Anna et al., *Phys. Chem. Chem. Phys.* **5**, 1790 (2003).

[20] S. Y. T. van de Meerakker et al., *Phys. Rev. Lett.* **94**, 023004 (2005).

[21] T. D. Hain, R. M. Moision, and T. J. Curtiss, *J. Chem. Phys.* **111**, 6797 (1999).

[22] J. van Veldhoven, H. L. Bethlem, and G. Meijer, *Phys. Rev. Lett.* **94**, 083001 (2005).

[23] B. Kuhn, *J. Chem. Phys.* **111**, 2565 (1999).

[24] D. M. Brink and G. R. Satchler, *Angular Momentum* (Clarendon Press, Oxford, 1993), 3rd ed.

[25] C. Ticknor and J. L. Bohn, *Phys. Rev. A* **71**, 022709 (2005).

[26] J. R. Alvarez-Idaboy et al., *J. Amer. Chem. Soc.* **123**, 2018 (2001).

[27] E. R. Hudson et al., *Eur. Phys. J. D* **31**, 351 (2004).

[28] R. Spence and W. Wild, *J. Chem. Soc.* **1**, 338 (1935).

[29] W. E. Henke et al., *J. Chem. Phys.* **76**, 1327 (1982).

[30] K. Shibuya et al., *J. Phys. Chem.* **83**, 940 (1979).